Agricultural and Forest Meteorology 347 (2024) 109896

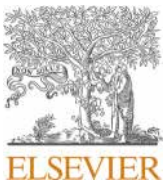

Contents lists available at ScienceDirect

Agricultural and Forest Meteorology

journal homepage: www.elsevier.com/locate/agrformet

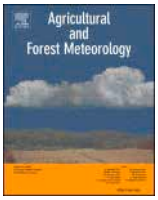

A new approach combining microwave heat pulse and infrared thermography for non-invasive portable sap flow velocity measurement

Hervé Louche [a], Annick Penarier [b], Philippe Nouvel [b], Bruno Clair [a], Christophe Coillot [c], Frédéric C. Do [d,e,*]

[a] LMGC, CNRS, University Montpellier, Montpellier, France
[b] IES, CNRS, University Montpellier, Montpellier, France
[c] L2C, CNRS, University Montpellier, Montpellier, France
[d] IRD, LMI IESOL, Centre ISRA-IRD de Bel Air, Dakar, Senegal
[e] Eco&Sols, CIRAD, INRAE, IRD, Institut Agro, University Montpellier, Montpellier, France

ARTICLE INFO

Keywords:
Microwave self-heating
Infrared camera
Heat wave
Contactless method
Water use

ABSTRACT

Xylem sap flow measurement is a key method to quantify plant water use and assess the responses to environmental conditions and climatic change. However, available methods are generally invasive and of limited portability. This paper presents a non-invasive approach called TIMFLOW that combines microwave heat pulse and infrared thermography, while having a high portability and versatility potential. The methodology was tested in laboratory conditions for black poplar (*Populus nigra)* stems of various diameters (10–45 mm) and for the known sap flow velocity range (10–100 cm h^{-1}). The heat pulse was generated by microwaves with a power amplifier supplying a bi-quad antenna at 2.45 GHz frequency located near the stem. The scene was filmed using a relatively low-cost light and compact InfraRed (IR) thermography camera. A stem temperature map was used to determine the heat pulse propagation velocity. The calculated heat velocity was highly correlated with the applied flow velocity with a unique relationship regardless of the diameter. The latter result confirms the equation of Marshall (1958) which links the sap velocity to the heat velocity with a vessel fraction of around 25 % within samples. The feasibility of outdoor measurements was also successfully tested. The assumed potentials and limitations of the proposed methodology are discussed. In summary, the study demonstrates the concept and validates, in woody stems, this new methodology for non-invasive portable sap flow velocity measurement.

1. Introduction

Over the last 30 years, sap flow measurements have been highly useful for quantifying water use and gaining insight into the water and energy balance of crops, orchards, tree plantations and natural forests (Poyatos et al., 2021). These measurements also provide tools for applied objectives to assess water requirement, often in combination with remote sensing. Several methods are available to measure sap flow in stems and trunks (Vandegehuchte and Steppe, 2013; Kumar et al., 2022). However, they are generally intrusive and of limited portability, while there is a substantial need for methodologies that can handle large sample sizes in order to monitor water-use heterogeneity in the field without a permanent setup. There is hence considerable demand for an efficient non-invasive portable method for measuring the sap flow rate in individual plants to supplement current methodologies.

Sap flow is mainly measured by indirect thermometric methods which deduce a flow variable from the convective effect of the flow on introduced heat. These methods can be classified into four main groups depending how they measure the convective effect, apply heat, monitor the sapwood temperature and calculate flow variables (the following references are not exhaustive): 1) Pulse methods (Swanson and Whitfield, 1981; Cohen et al., 1981; Burgess et al., 2001; Vandegehuchte and Steppe, 2012; Forster, 2020), which measure heat transfer between points with inserted needles, resistive heat pulses and mainly deterministic calculations; 2) dissipation methods, which measure heat dissipation at a given point with inserted needles, empirical calibration, constant heating (Granier, 1985) or transient heating (Do and Rocheteau, 2002); 3) field methods (Nadezhdina et al., 2012), which measure the shape change of a continuous heat field in the sapwood with inserted needles and empirical calibration; and 4) balance methods, which

* Corresponding author at: IRD, LMI IESOL, Centre ISRA-IRD de Bel Air, Dakar, Senegal.
E-mail address: frederic.do@ird.fr (F.C. Do).

https://doi.org/10.1016/j.agrformet.2024.109896
Received 16 July 2023; Received in revised form 10 January 2024; Accepted 14 January 2024
Available online 29 January 2024

measure the energy balance across the whole stem (Sakuratani, 1981; Steinberg et al., al.,1989) with an external heating sheath, or across a wood section with inserted plates (Cermak et al., 1973), and mainly with deterministic equations. The latter family is the only one that measures the sap flow rate, while the others measure the sap flux velocity or density. All these methods have advantages and disadvantages and may be chosen according to the objective, plant material, experimental design, cost, available energy and users' experience.

Amongst these thermometric methods, the stem heat balance method is likely the most portable. However, external heating requires high power to cross the bark tissue and reach the xylem. This has negative impacts on energy consumption and bark health, thereby limiting the application of this method to small stems and short measurement campaigns. Moreover, the calculation is very sensitive to variability in the contact between the probe sheath and the wood.

Only a few instruments offer alternative perspectives towards portability. Nuclear magnetic resonance spectroscopy (NMR) and imaging (MRI) techniques, which are widely used for medical diagnosis, are attractive. Several methods and tools have been developed to measure sap flow in plants (Kumar et al., 2022). The main difficulty in MRI sap flow measurement is to be able to discriminate stationary from mobile water molecules (i.e. sap flow). The historical method can image moving water molecules based on a magnetic field gradient, but it requires complex data processing (Van As et al., 1984; Windt et al., 2006). A recent method, which may be easily conducted using commercial MRI, allows measurement of low sap flow velocity and reverse flow (Buy et al., 2018). Some authors have attempted to perform outdoor MRI or NMR experiments (Nagata et al., 2016; Sidiboulenouar et al., 2018). In spite of their potential, these approaches still require heavy instrumentation, so they are currently unsuited for field studies.

Combining contactless heat pulse and infrared thermography imaging is another attractive avenue for mobile sap flow measurement which has yet to be explored in detail. Thermal imaging has been developing since the 1970s in many industrial fields as well as medical fields. Spatiotemporal resolution, initially limited by the use of single detector cameras, has greatly improved with the advent, in the early 2000s, of cameras with detector arrays which allow the acquisition of high frequency images with good resolution. This type of imaging has been widely used in the field of mechanics of materials to study thermo-mechanical coupling (Chrysochoos, 2012). Thermal imaging only provides access to surface temperatures. Furthermore, due to conduction and thermal inertia phenomena, these thermal effects are generally spatiotemporally diffuse. In order to analyze the spatiotemporal aspects of these thermal effects, methods have been developed to estimate the heat sources and causes of such surface temperature variations. The method proposed by Chrysochoos and Louche (2000), which is limited to thin samples, enables estimation of 2D heat sources from thermal surface images. Through this method, the heat dissipation of mechanical power supplied to the sample could be studied in many classes of materials (steels, aluminum alloys, polymers, elastomers, shape memory alloys, etc.). Thermal imaging applications in the medical field are also worth mentioning (Diakides et al., 2008). This type of imaging enables the analysis of blood flow in veins (Ratovoson et al., 2011) or of thermoregulation disturbances induced by diabetic complications (Serantoni et al., 2021). For sap flow applications, the pioneering work of Anfodillo et al. (1993) highlighted the benefits of combining heat pulse induced by a resistive wire and thermal imaging on the opposite side to produce qualitative information on the sap movement pathway according to plant species and individuals. A similar approach was implemented by Tributsch et al. (2006) and Nadezhdina et al. (2012) who used infrared images of trunks that had been deeply scraped on the side opposite that of an inserted constantly heated needle to assess the positioning of surrounding needle sensors in the heat field deformation method (Nadezhdina et al., 1998). On small herbaceous stems, Bauerle et al. (2002) successfully tested an external device combining a heat pulse from laser diode and point infrared thermometers. Helfter et al. (2007) studied the application of an external device to small ligneous stem that combined laser and infrared thermography heat pulses, while also applying heat pulse theory. In spite of the interesting results obtained, the author noted the potential difficulty in applying their method to stems of larger diameter (>12 mm). Hence, microwave heat pulses could offer a more versatile external method in which the signal could be able to cross bark tissue and induce heating of well hydrated xylem vessels in larger stems. The use of this technology was mentioned in the book of Kozlowki and Paillardy (1997), but there were no specific references and no further developments have since been published. Moreover, the sap flow density is known to have a radial profile in large stems and trunks, with maximum values in the outer xylem vessels (Berdanier et al., 2016), which could be detected by surface IR imaging.

The proposed new approach involves combining microwave heat pulse and infrared thermography to obtain a non-invasive portable measurement of sap flow velocity in stems. This study was carried out to highlight the feasibility of the concept and validate the methodology in the laboratory with woody stems of different diameters. The first step was to induce a heat pulse by an external microwave device. We assumed a significant heat pulse regardless of the stem diameter within a diameter range manageable in the laboratory. The second step was to calculate the heat velocity via thermal imaging. The final step was to analyse the relationships between a controlled flow rate and the calculated heat velocity. We expected to obtain significant relationships with minimal stem diameter effects for the same species.

2. Methods

This part presents the TIMFLOW (Thermal Imaging and Microwave for quick and mobile assessment of sap flow) setup, combining a microwave heating and thermal imaging (Fig. 1). After a short presentation of the theoretical basis, we will describe these setups, the tree material and flow conditions. The outdoor conditions are finally given in the last part of this section.

2.1. Theoretical basis

The theoretical equations used to relate the sap flow and heat velocity in xylem are derived from the theory of conduction and convection of heat in porous material (Marshall 1958).

Marshall presented a first model to predict the link between the heat pulse velocity (V_{hp}) carried by sap and the sap flow (u) in the conductive vessels:

$$V_{hp} = au\frac{\rho_s C_s}{\rho C} \quad (1)$$

where ρ, C, ρ_s and C_s are, respectively, the volumetric mass density and the heat capacity of the wet wood and the sap (index s). Parameter a concerns the fraction of conductive area of the specimen. It can be estimated by the ratio $a = \frac{A_{ves}}{A_{sw}}$, where A_{ves} is the vessel area carrying sap and A_{sw} the average sapwood area calculated by: $A_{sw}=\frac{\pi}{4}(d_{sw}^2 - d_{\varphi}^2)$, where d_{sw} and d_{wp} are, respectively, the sapwood diameter measured after removing the bark and the wood pith diameter. The demonstration of the relation (1) was based on a 1D hypothesis in an infinite medium, assuming that the sap velocity was uniform in each vessel, and that the heat was transported by convection by the sap only in the axial direction.

2.2. Microwave heating setup

The water absorption spectrum includes several water absorption windows centered on 2.45 GHz, 22 GHz, 183 GHz. The use of a high frequency system has a better spatial resolution but on the other hand a higher cost, while the components have low available power. For lower frequencies, the wave penetration depth is greater, and the device cost is

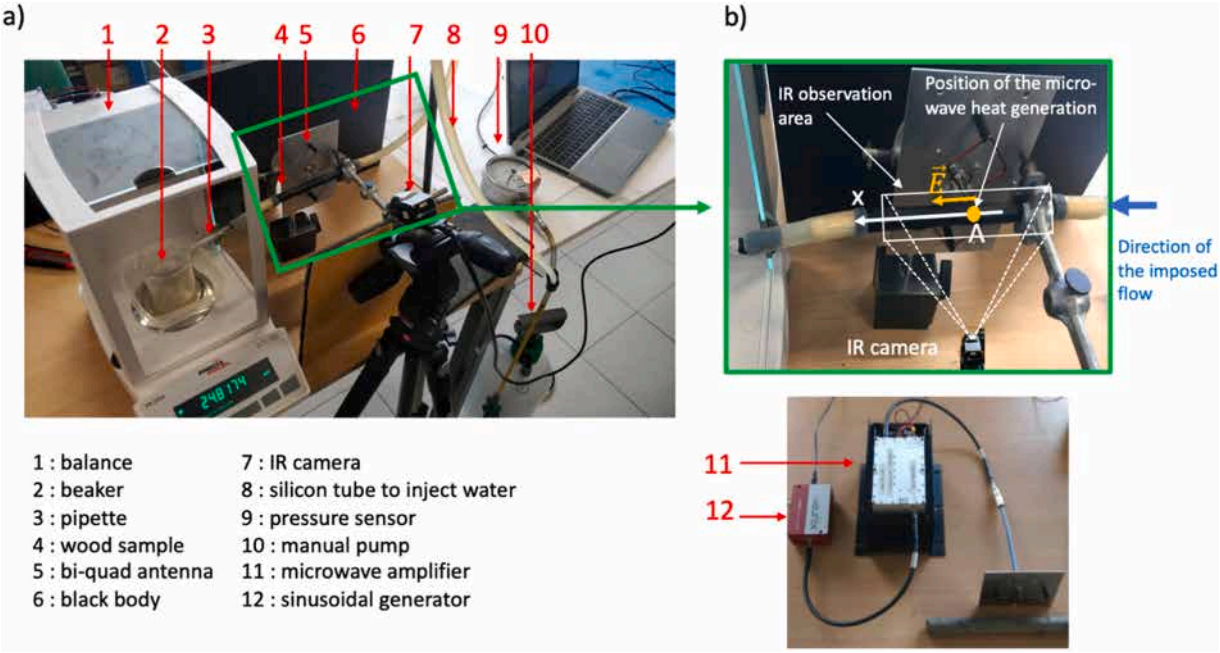

Fig. 1. Laboratory setup: (a) General view. (b) Close-up showing the IR observation area, the position (point A) of the microwave heat generation, the E field direction and the direction of the imposed flow along x direction. The bottom picture summarizes the microwave setup (generator + amplifier + bi-quad antenna).

lower. For this last reason, the working frequency was set at 2.45 GHz. The microwave device included a commercial high-frequency generator (Vaunix LMS 402D) with an input power of - 7 dBm at 2.45 GHz. It supplied a 50 dB microwave power amplifier (mini-circuit ZHL-30W-262-*S*+). Consequently, the available output power on a matched dipole was about 43 dBm (20 W). The power amplifier output signal supplied the microwave antenna (cf. Fig. 1b) which produced the self-heating of the exposed tissue. The antenna was a wired bi-quad with a resonance frequency of 2.45 GHz. The quad antenna was designed with a copper wire length corresponding to the wavelength of the electromagnetic wave in vacuum at 2.45 GHz (i.e. about 12.24 cm). The combination of two quads in series formed an antenna array (Arguelles et al. 2017). This was called bi-quad or double quad antenna. This wire was positioned under a reflector plane with a size of 160 mm x 100 mm (Fig. 1a). The combination of the two quads and the aluminium reflector plane enabled a higher gain than the quad alone, thereby improving the heating. The antenna had a gain of about 11 dB and a 3 dB beamwidth of 20°

2.3. IR thermography setup

The IR camera chosen in this project was a SmartIR640 (DeviceAlab, Grenoble, France) IR camera, with a long wave sensitivity (LWIR 8–14 mm). This choice was a trade-off between its relative low cost and its technical specifications. The IR camera had a resolution of 640×480 pixels, a maximal frame rate of 30 Hz and a thermal resolution (NETD) of 50 mK. The thermal radiation emitted by the wood sample surface was converted to a signal, often called a thermosignal, proportional to the thermal radiation and coded at 14 bits (i.e. 16,384 digital level [DL]). A calibration procedure using a laboratory blackbody is usually necessary to obtain temperature fields from the thermosignal. However, in the present study, this procedure was not necessary as the thermosignal fields were sufficient to estimate the heat pulse velocity. The calibration law linking the thermosignal and the surface temperature was not perfectly linear. However, in order to give a magnitude of temperature variations, one can accept a linearization of it. In these specific test conditions, a change of 1 K corresponded to a change of about 588 DL for the thermosignal. The IR camera had a length of 50 mm, a weight of 140 g and was powered by a laptop USB port connexion. Compared to more expensive IR cooled sensors, the uncooled microbolometer sensors of this camera led to significant spatial noise and thermosignal temporal drift in each pixel (due to self-heating) which had to be managed. This was achieved by subtracting a thermosignal obtained at a reference point from the thermosignal fields in the test area. The reference point was located outside this area, with an assumed constant temperature (i.e. constant thermosignal).

2.4. Tree material

Black poplar (*Populus nigra*) stems were sampled in the neighbourhood of the lab (Montpellier, France). As soon they were cut, the ends were sealed with parafilm. The tests were carried out within 30 min after sampling. A total of 13 stems of about 200 mm length with diameters ranging from 10 mm to 50 mm were tested (see Table 1).

After the flow testing, the samples were stored in a mixed ethanol/water solution to study their porosity under a microscope (see example in Fig. 2). Thin sections (around 18 μm thickness) were prepared with a sliding microtome and stained with safranin. Images of the sections were obtained through a microscope and anatomical measurements were performed with ImageJ image analysis software. All sapwood areas A_{sw} were measured for each sample. For all samples, a mean value of 2 mm was assumed for the pith diameter. For six samples (numbers 4, 5, 7, 8, 9, 10), the vessel areas A_{ves} were measured to compute the fraction of conductive area a (Table 1).

2.5. Flow testing conditions in laboratory

Before processing, the samples were recut at both ends under water with a brand-new razor blade. An aqueous solution of ultrapure water with antiseptic (10 mM KCl) and stabilizer (1 mM $CaCl_2$), was used for the water flow circulation. The solution was injected in the basal part of the sample using a manual pump controlling the solution input pressure. Pressures between 0.1 to 1.2 bars were applied, depending on the sought flow velocity, i.e. between average values of 10 to 100 cm h^{-1} regardless of the diameter, while dividing the flow rates by the whole sapwood area. A balance (Precia Molen XB220A, France) regularly measured the

Table 1
Poplar stem samples tested (N = 13). D_{sw} is the sapwood diameter after removing bark; NA = not available.

Sample number	Output diameter *Do* (mm)	Sapwood diameter *Dsw* (mm)	Fraction of conductive area *a* (%)	Imposed flow Qm (g.s-1)
1	12.6	10	NA	0.00370; 0.0140;0.0250
2	12.8	9.4	NA	0.0000; 0.0000; 0.0000; 0.0000; 0.0000; 0.0187; 0.00640; 0.0107
3	12.64	9.6	NA	0.0140; 0.0000; 0.0105; 0.0212; 0.00690
4	20.25	17.1	24.9	0.0000;0.1608;0.1092; 0.0890
5	22	18	19.5	0.0478; 0.0319; 0.0316; 0.0143
6	18.3	15.1	NA	0.0615; 0.0474; 0.0304; 0.0264; 0.00640
7	14.7	12	19.9	0.0825; 0.0639; 0.0225; 0.0187; 0.00690; 0.0122
8	33	29.3	20.1	0.1657; 0.121; 0.0521; 0.0679; 0.0373; 0.0216; 0.0376; 0.0785; 0.0767
9	27	23	16.6	0.0888; 0.0778; 0.0433; 0.0339; 0.0164; 0.0137
10	41	35.6	15.7	0.0366; 0.0871; 0.0608; 0.115; 0.0286; 0.0139; 0.0000
11	44.5	39	NA	0.0869; 0.0606; 0.0680; 0.0765; 0.0750; 0.0622; 0.0615; 0.0557; 0.0370; 0.0376
12	40.5	33.5	NA	0.103; 0.137; 0.150; 0.141; 0.0000
13	44.7	40	NA	1.41; 0.720; 0.512; 0.484; 1.36; 1.09; 0.485; 0.558; 0.377; 0.0000

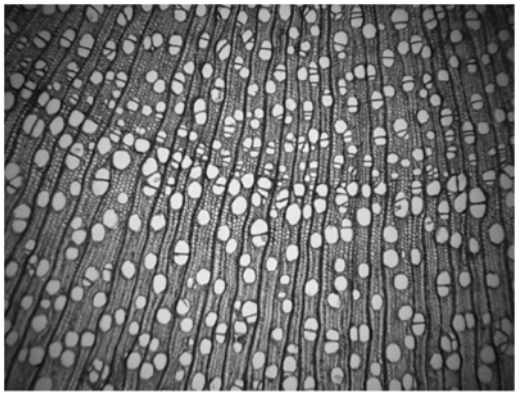

Fig. 2. Thin section of a poplar wood sample showing the numerous vessels devoted to water transport.

mass of the output solution, thereby highlighting the temporal variations in the mass flow Q_m (in g s^{-1}) (Fig. 1.a). Table 1 summarises the flow rate values and metrics necessary for sap velocity calculations.

2.6. TIMFLOW setup

The wood sample was positioned parallel to the *E* field of the antenna at a distance of 3 to 10 mm. Preliminary experiments with an IR camera and thermal-electrical finite element modelling (not presented in this paper) showed that the wood sample was mainly heated on the back side in small stems (10 to 20 mm) and on the front side in medium stems (30–45 mm). Thus, the spatial configuration antenna/camera was adapted to the situations. An example for a small stem configuration with the antenna on the back side is given in Fig. 1b.

The thermosignal of the sample surface was recorded at a *f_IR* frame rate (5 Hz), over a time period *t_heat* of about 4 min, including three stages. During the first one, with a duration about 10 s, the initial radiation state from the scene was recorded to have a reference state. During the second stage, the microwave system was switched "ON" for 10 s to 1 min according to the stem diameter to induce visible local heating of 2 to 4 °C. Finally, a last recording stage enabled monitoring of heat transport by the sap flow over the remaining time. All the heat pulse loadings imposed by the microwave system were performed with the same power (20 W). The spatial resolution (pixel size) of the thermal images was 0.2 mm.

2.7. Outdoor conditions

The setup was tested in outdoor conditions on living poplar trees with diameters ranging from 12.8 to 103 mm. The same setup as the one previously described was implemented outside. Precautions were taken to avoid direct sunlight on the stem by using a shade cloth. An example of this test is given later in Fig. 7a, where a trunk of diameter 103 mm was tested. A hot spot (point H) was first generated by the antenna, which was later removed by a rotation *a* to observe the thermal radiation at the surface with the infrared camera.

3. Results and discussion

3.1. Heat pulse velocity assessment

The findings are presented according to three tests conducted on the same small stem sample 1 (*Do*=12.6 mm) at the following flow rates Q_m (0.00370; 0.0140; 0.0250 g s^{-1}), respectively denoted 1_a, 1_b and 1_c.

The images in Fig. 3a illustrate, for a medium velocity (test 1_b), the thermosignal at different times ranging from 40 s (image number 200) to 160 s (image number 800), with a 20 s step between images. These series of images clearly showed that the heat pulse generated by the microwaves was moving downstream (right direction) and carried by the water flow. The second observation was the reduction of its amplitude due to transport and heat exchange with the surroundings. The same analysis was done for the different axial profiles, plotted at the same time in Fig. 3b. Finally, the juxtaposition of the different axial profiles for each image led to the spatiotemporal image reported in Fig. 3c. The heat pulse was moving regularly in the *x* direction (bottom) at constant velocity, as indicated by the black arrow.

A qualitative estimation of its velocity was obtained from this last representation, but a more precise value was computed through estimation of the axial position in pixels of the thermal pulse (peak) of each axial profile. The peak position i_{max}, where the DL was maximum, was detected by a local least mean square approximation $\widetilde{DL}$of the thermosignal, with a polynomial function of degree 2:

$$\widetilde{DL}(i,k) = a_k i^2 + b_k i + c_k, \tag{2}$$

where a_k, b_k, c_k are the coefficients for the current image number k at pixel position i. The peak position $i_{max,k}$ for image k is then given by:

$$i_{max,k} = \frac{-b_k}{2a_k}. \tag{3}$$

Temporal variations in $i_{max,k}$ are plotted in Fig. 3d for image numbers k = 250 to 700, i.e. after the microwave loading (see also the limit of the black arrow in Fig. 3c). As already noted, the peak position variation patterns were more or less linear, leading to a constant velocity, compatible with the constant flow imposed. The fit with a linear approximation superimposed on this plot allowed us to estimate a heat pulse velocity of V_{hp}=*57.6* cm h^{-1}.

The results obtained on the same sample 1 in two contrasted imposed flow (tests 1_a and 1_c) are given in Fig. 4. The spatiotemporal graphs

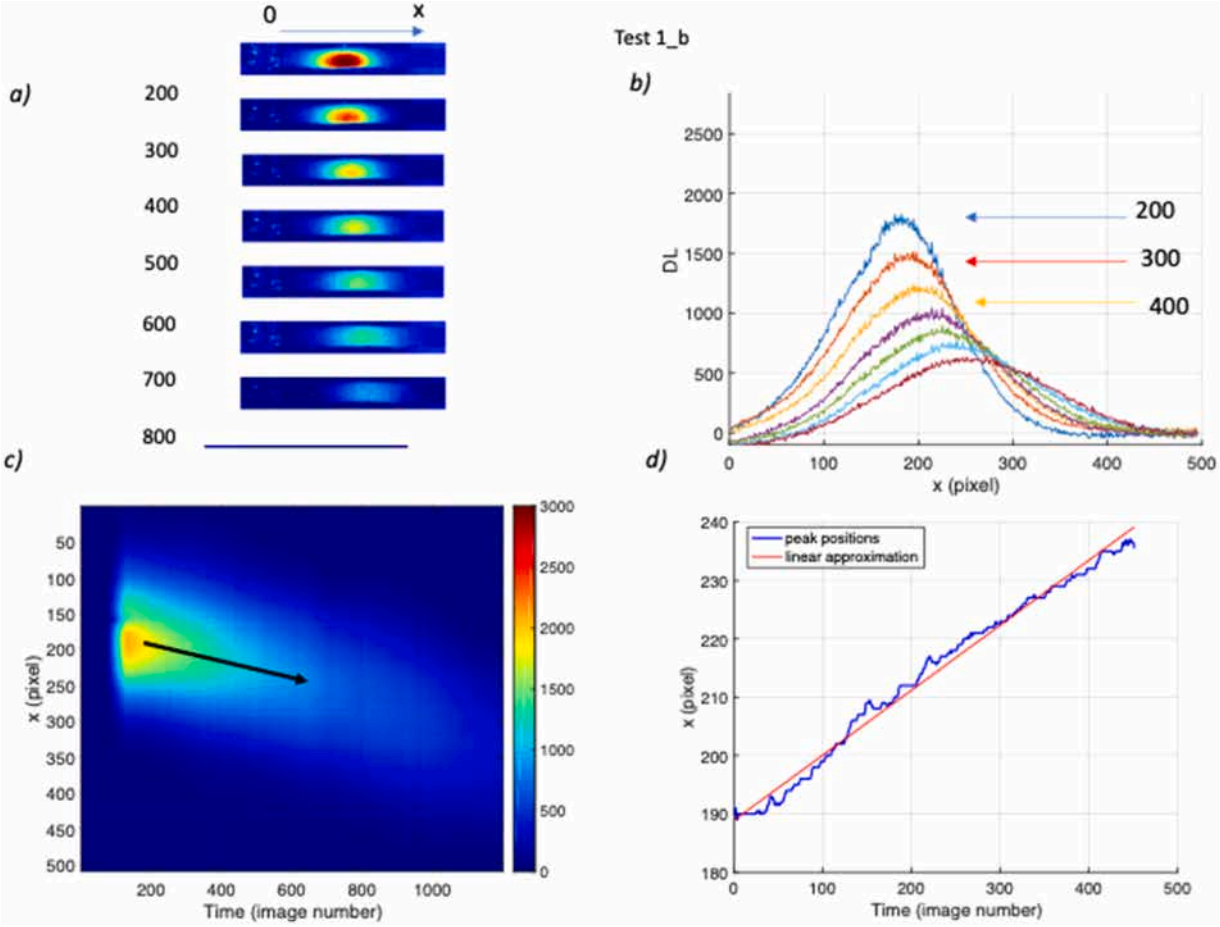

Fig. 3. Thermal images and heat pulse analyses for a small stem (sample 1, D_0=12.6 mm) and a mean flow velocity of 57.6 cm h^{-1} (test 1_b; imposed flow of 0.0140 g s^{-1}). a) Example of seven thermal radiation images (number 200, 300,…, 800) showing the propagation and attenuation of the heat front. b) thermal radiation profiles along x direction at the same times. c) spatiotemporal variations in thermal radiation measured at the sample surface. d) Temporal variations in the peak position in pixel $i_{max,k}$ and its linear approximation.

were clearly different between flow rate conditions, with the overall slope (black arrow) representing the average heat velocity. For a low imposed flow (test 1_a), the heat pulse was more intense and moving slowly. In the case of a higher imposed flow (test 1_c) the heat pulse intensity was lower and rapidly decreasing due to the water transport.

The heating zones exhibited a maximal temperature increase between 2 and 5 °C, with a spatial extension of about 50 pixels, i.e. 10 mm. For example, for test 1_b, at image number 200, the peak amplitude was about 1800 DL for the thermosignal, leading to a temperature increase of about 3 °C at this location (Fig. 3b).

3.2. Linking the heat velocity to the controlled flow

Based on knowledge of the imposed mass flow rate Q_m, the following relation was used to compute the average sap velocity u_{av} in the sapwood area:

$$u_{av} = \frac{Q_m}{\rho A_{sw}}. \quad (4)$$

When the vessel area A_{ves} was taken into account, the average sap velocity in the vessels u was estimated with:

$$u = \frac{Q_m}{\rho A_{ves}} = \frac{u_{av}}{a}. \quad (5)$$

The measured heat pulse velocities V_{hp} are plotted versus the average sap velocity u_{av} calculated according to relation (4), for all data of Table 1 (Fig. 5).

A high linear correlation was obtained (R^2=0.949; RMSE=12.83) without apparent influence of stem diameters. The comparison with a similar relationship assessed by Helfter et al. (2007) for a narrow range of very small twig diameters (3–4 mm) enhanced the significance of this result with stems ranging from 12 to 45 mm. The origin of the linear fit was (0, 1.75), indicating that the heat pulse displacement was negligible when the flow rate was zero, suggesting that the velocity measurement was absolute. According to the slope value, the heat pulse velocity appeared to be slightly higher than the average sap velocity in the sapwood area. Indeed, the sapwood area overestimated the active vessel area A_{ves} and led to an underestimation of the average sap velocity u_{av}.

To have a more realistic relationship between heat pulse velocity and sap velocity, a new figure was plotted for the six samples (numbers 4, 5, 7, 8, 9, 10), where the fraction a of the conductive area was measured (Fig. 6). The heat pulse velocity V_{hp} was then compared to the sap velocity u in the vessels with relation (5).

The strength of the relationship was slightly improved (R^2=0.972; RMSE=11.5) through both the increase in the R^2 and the decrease in the RMSE (R^2=0.949 and RMSE=12.8 were obtained for the same subsampling, as shown in Fig. 5). The origin was still close to zero and the sap velocity was about fourfold that of heat pulse velocity. This value could be compared to that given in Marshall 1958, where the sap flow velocity was threefold that of the heat pulse velocity in conifers.

3.3. Outdoor testing

As a demonstration of the feasibility in outdoor conditions, in this section we show an example of a typical result obtained in a living poplar trunk of 103 mm diameter (Fig. 7a). Three thermal radiation images, recorded at 15/4 Hz frequency, after local microwave heating

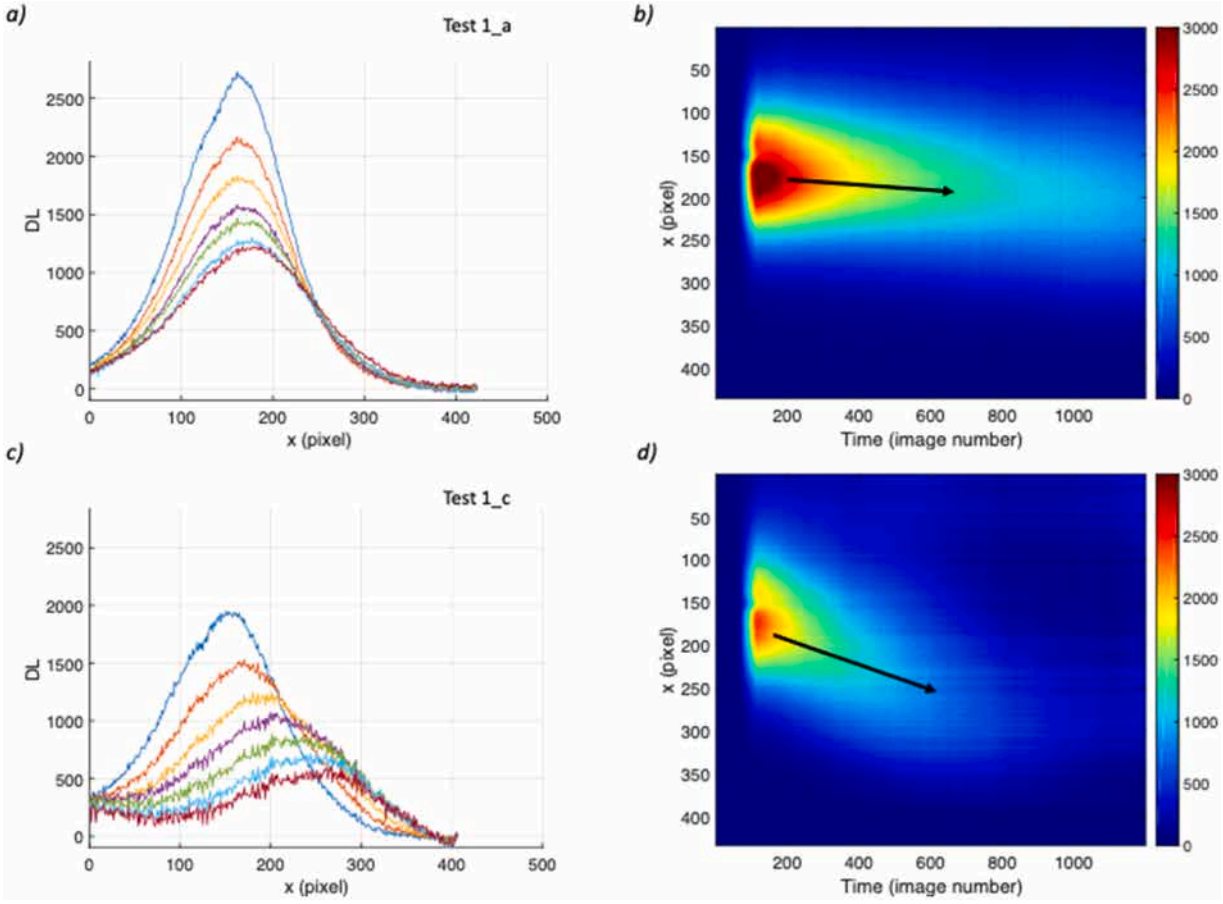

Fig. 4. Heat pulse diagrams for contrasted imposed flow rates. Test1_a: low imposed flow 0.0037 g s^{-1} (mean sap velocity 14.4 cm h^{-1}); a) thermal radiation profiles, along x direction, at image numbers 200, 300,… to 800 (respectively 40, 60,…, 160 s) and b) spatiotemporal representation of the thermal radiation measured at the sample surface. Test 1_c: high imposed flow (0.0250 g s^{-1}; mean sap velocity 104.4 cm h^{-1}); same description as in a and b.

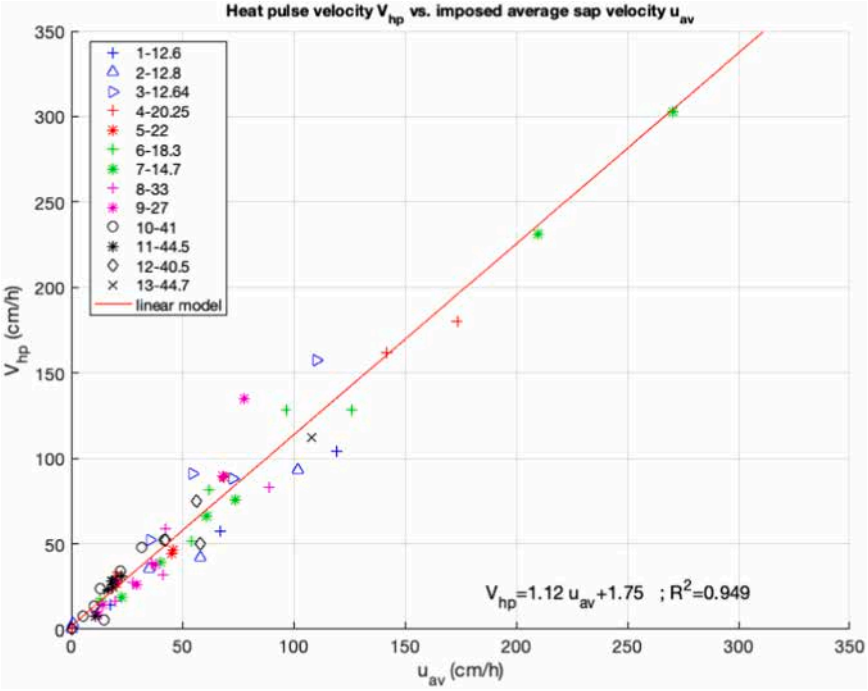

Fig. 5. Assessed heat pulse velocity V_{hp} versus average sap flow velocity u_{av} in the sapwood for the 13 stem samples. ($n = 82$).

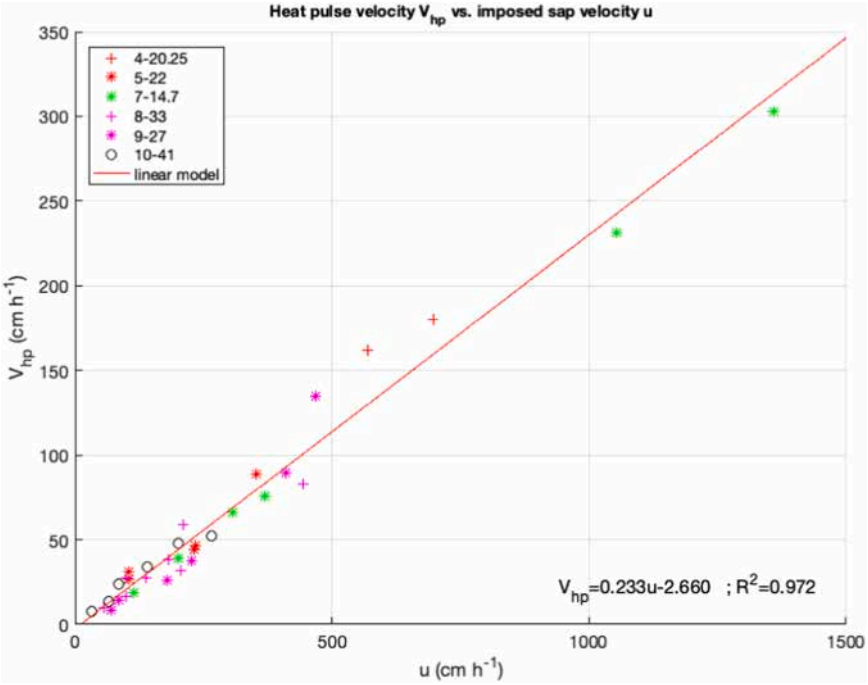

Fig. 6. Assessed heat pulse velocity V_{hp} versus the sap flow velocity u in the vessels (n = 34).

around point H, are plotted in Fig. 7b. A time of 80 s separated these images. The heat pulse propagation in x direction (upwards) and its attenuation were clearly visible. The thermal radiation profiles in x-direction shown in Fig. 7c confirmed this propagation pattern and allowed us, as explained in the previous section, to calculate the heat wave velocity. Finally, the spatiotemporal representation plotted in Fig. 7d showed that this speed was constant throughout the propagation in the observed area. A heat wave velocity of 18.7 cm h^{-1} was measured in this outdoor test.

3.4. Trade-offs and challenges

The results provided experimental proof of the TIMFLOW concept of a non-invasive device combining a microwave stimulus and infrared thermography and they validated the methodology in the laboratory in woody stems. In the association with infrared thermography, the results highlight the interest of the microwave stimulus versus laser pulse (Bauerle et al., 2002; Helfter et al., 2007) to induce internal heating in large stems. Infrared thermography also offers a robust heat wave velocity measurement method. However, the potential advantages of this new approach over existing thermometric methods must be balanced against the trade-offs discussed hereafter. First, TIMFLOW portability enables users to obtain intermittent measurements in several plants but it cannot be used for continuous monitoring with the current prototype. TIMFLOW can also be used with a larger range of stem diameters than existing methods, with the only change concerning heating time. In heat pulse and thermal dissipation methods, the needles should be adapted to the xylem width and cannot be applied to very small stems. In stem heat balance methods, the device should be adapted to the stem diameter range and cannot be applied to large stems or trunks. However, stem heat balance methods have the advantage of being able to directly measure the sap flow rate, while other methods, including TIMFLOW method, measure the sap flow velocity or density and require sapwood area data to estimate the sap flow rate. Moreover, with TIMFLOW, the sapwood area, spatially integrated by the measured heat velocity, is not clearly known. The strength of the relationship between the heat velocity and the flow velocity, deduced from imposed flow rates, highlighted good spatial integration of the whole sapwood area. However, the experiment concerned relatively low diameters. We expected a reduced detection area in larger stems. As in existing thermometric methods with needle insertion (Vandegehuchte and Steppe, 2013), measurements at several angles should be considered with the TIMFLOW system and physical modelling can provide reliable information on the spatialized heating pattern. The representativeness is also related to the radial profile of sap flow density, which is known to change according to species, seasons, and water constraints despite its overall decreasing trend towards inner xylem (Berdanier et al., 2016). This radial distribution of sap velocity cannot be measured with the TIMFLOW method while the radial profile can be assessed with conventional methods using needles. By contrast, TIMFLOW is expected to improve the local measurement accuracy by overcoming the effects of probe insertion or of the heterogeneity of the probe-wood contact (needle or sheath), and also by limiting the tissue reaction. Management of the wounding effect due to needle insertion is challenging in both heat pulse (Swanson and Whitfield, 1981) and dissipation (Wiedemann et al., 2016) methods. These accuracy improvements are key issues to estimate zero, low or reverse sap flow.

One common limitation of methods with external heating such as TIMFLOW or the Stem Heat Balance is that the observed heat velocity is the result of the combination of two sap flows, in both phloem and xylem tissues. Although the phloem sap flow volume could be expected to be much smaller compared to the xylem sap flow. Moreover, it is possible to estimate the influence of the phloem sap flow by locally removing the bark before a second measurement (Helfter et al., 2007).

As shown in our results, the vessel sapwood fraction must be considered when assessing the relationship between heat velocity and sap velocity. Moreover, the hypothesis of only 1D (axial) heat transfer (Eq. (1)) is relative and may be challenged according to the wood type and species (Vandegehuchte and Steppe, 2013). The development of a generic model to estimate the total flow is a challenge which has likely to consider the species, the age or the size of the conducting cells.

With a view to applications, potential TIMFLOW users are forestry professionals and large-scale orchard or vineyard managers who cannot afford to continuously monitor as many trees as they would like. Yet it is interesting for researchers to explore the sap flow velocity, direction (downward, upward) or zero achievement in different organs and

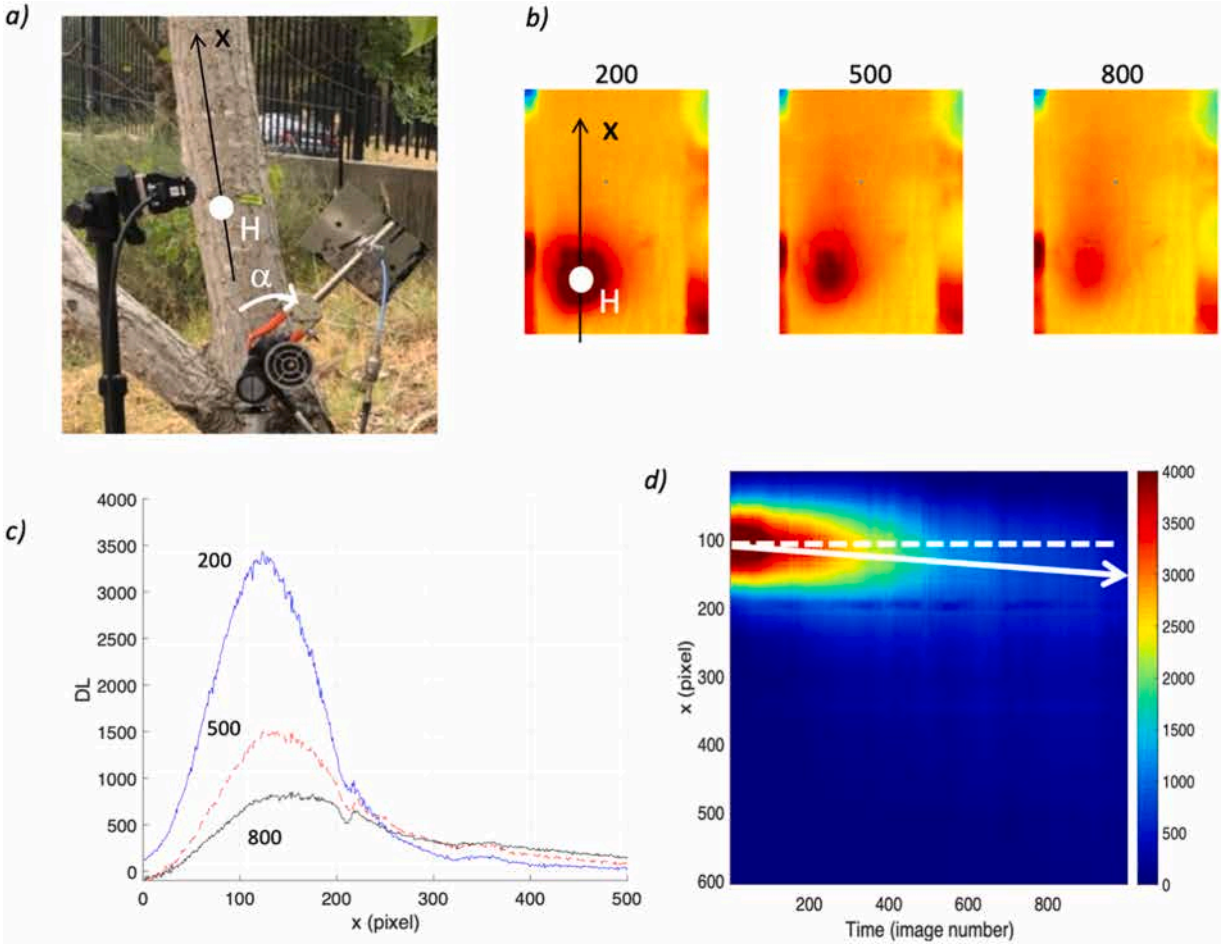

Fig. 7. Example of an outdoor test. (a) experimental setup on a poplar tree trunk (103 mm diameter) showing the microwave excitation point H (after a rotation a of the antenna) and the infrared camera recording heat propagation in x direction. (b) Example of three thermal radiation images (number 200, 500, 800) showing the propagation and attenuation of the heat front. (c) thermal radiation profiles along x direction, at the same times. (d) spatiotemporal variations in the thermal radiation measured at the sample surface, showing the heat pulse propagation pattern (white arrow).

between species without a fixed setup. Finally, according to the scaling of the Technology Readiness Level (EARTO 2014), the results indicated that level 3 (experimental proof of the concept) and level 4 (validation of the methodology in laboratory conditions) had been achieved. The next development steps will be to test the current TIMFLOW prototype in various outdoor conditions and to elaborate a V2 adapted to operational conditions (TRL 5 and 6). The current system is already portable and all of the devices in our system are powered by an external 12 V battery or through a laptop USB port. Outdoor experiments are under way and several technical aspects are being tested to improve the efficiency and mobility of the device. The current max power used is high (20 W) and should be reduced by optimizing the antenna for near field applications. The size and cost of the frequency generator are also an issue. Theexternal temperature measurement device is also under evolution . In association with a microwave heating system, two orientations are considered here: a mobile device using a light camera for thermography and a low-cost static device based on a 1D array of infrared detectors.

4. Conclusion

The need for a non-invasive portable sap flow measurement method has been addressed. Here we have presented a new non-invasive approach called TIMFLOW that combines microwave heat pulse and infrared thermography, which has a high portability and versatility potential. The results demonstrated the feasibility of the concept and validated the methodology in the laboratory with woody stems of different diameters. The laboratory testing conditions in a highly porous woody species were obviously ideal and several issues were discussed for the overall applications. The advantages and drawbacks relative to currently used methods have been presented. There are trade-offs when it comes to choosing between a portable tool and a device designed for continuous monitoring. The TIMFLOW concept may interest a new array of professional users needing, for instance, to check sap flow in large-scale fields or forests. However, it can also be of interest to researchers because it offers new applications to a broad range of tree organs: stems, trunks, branches and coarse roots. Finally, for next development steps, the main issues identified are: 1) to achieve a power reduction through antenna optimization; 2) to enhance the versatility between mobile and static devices; 3) to improve the compactness of the device; and 4) to assess a generic model to estimate the sap flow rate. These issues are currently being studied and the expertise on antenna designs and current thermometric methods should help to accelerate the process.

CRediT authorship contribution statement

Hervé Louche: Writing – review & editing, Writing – original draft, Methodology, Formal analysis, Data curation. **Annick Penarier:** Writing – original draft, Methodology, Formal analysis, Data curation, Conceptualization. **Philippe Nouvel:** Writing – original draft, Methodology, Formal analysis, Data curation, Conceptualization. **Bruno Clair:** Writing – original draft, Methodology, Formal analysis, Data curation,

Conceptualization. **Christophe Coillot:** Writing – review & editing, Writing – original draft, Methodology, Formal analysis, Data curation, Conceptualization. **Frédéric C. Do:** Writing – review & editing, Writing – original draft, Methodology, Data curation, Conceptualization.

Declaration of competing interest

The authors declare that they have no known competing financial interests or personal relationships that could have appeared to influence the work reported in this paper.

Data availability

Data will be made available on request.

Acknowledgments

Msc Students from Montpellier University: Hanane Guerouaz, Lucien Masse, Paul Mohammadi, Achille Majzels, Lucas Descazaux.

This work was supported by the CNRS 2020 "Climate Change" program. The authors would like to also thank the Region Occitanie/ Pyrénées Méditerranée through the HERMES platform for partial funding of this research.

The experiment has also received partial funding from the Sustain-SAHEL project under the European Union Horizon 2020 research and innovation program, grant agreement No 861974.

References

Anfodillo, T., Sigalotti, G.B., Tomasi, M., Semenzato, P., Valentini, R., 1993. Applications of a thermal imaging technique in the study of the ascent of sap in woody species. Plant Cell Environ., 16, 997–1001.

Arguelles, A.Z., 2017. Super high frequency reflective biquad antenna. In: Proceedings of the IEEE International Symposium on Antennas and Propagation & USNC/URSI National Radio Science Meeting, pp. 2205–2206.

Bauerle, W.L., Whitlow, T.H., Pollock, C., Frongillo, E.A., 2002. A laser-diode-based system for measuring sap flow by the heat-pulse method. Agric. For. Meteorol. 110, 275–284.

Berdanier, A.B., Miniat, C.F., Clark, J.S., 2016. Predictive models for radial sap flux variation in coniferous, diffuse-porous and ring-porous temperate trees. Tree Physiol. 36, 932–941.

Burgess, S.S.O., Adams, M.A., Turner, N.C., Beverly, C.R., Ong, C.K., Khan, A.A.H., Bleby, T.M., 2001. An improved heat pulse method to measure low and reverse rates of sap flow in woody plants. Tree Physiol. 21 (9), 589–598.

Buy, S., Le Floch, S., Tang, N., Sidiboulenouar, R., Zanca, M., Canadas, P., Nativel, E., Cardoso, M., Alibert, E., Dupont, G., Ambard, D., Maurel, G., Verdeil, J.L., Bertin, N., Goze-Bac, C., Coillot, C., 2018. Flip-flop method: a new T1-weighted flow-MRI for plants studies. PLOS One 13 (3), e0194845. https://doi.org/10.1371/journal.pone.0194845.

Cermak, J., Deml, M., Penka, M., 1973. A new method of sap flow rate determination in trees. Biol. Plant. 15, 171–178.

Chrysochoos, A., Louche, H., 2000. An infrared image processing to analyse the calorific effects accompanying strain localisation. Int. J. Eng. Sci. 38 (16), 1759–1788.

Chrysochoos, A., 2012. Infrared thermography applied to the analysis of material behavior: a brief overview. Quant. InfraRed Thermogr. J. 9 (2), 193–208.

Cohen, Y., Fuchs, M., Green, G.C., 1981. Improvement of the heat pulse method for determining sap flow in trees. Plant Cell Environ. 4, 391–397.

Do, F., Rocheteau, A., 2002. Influence of natural temperature gradients on measurements of xylem sap flow with thermal dissipation probes. 2.Advantage and calibration of a non-continuous heating system. Tree Physiol. 22, 649–654.

Diakides, N.A., Bronzino, J.D., 2008. Medical Infrared Imaging. CRC Press.

EARTO, 2014. The TRL scale as a research & Innovation policy tool, EARTO recommendations. European Association of Research and Technology Organisations https://www.earto.eu. 17 p.

Forster, M.A., 2020. The importance of conduction versus convection in heat pulse sap flow methods. Tree Physiol. 40, 683–694.

Granier, A., 1985. Une nouvelle méthode pour la mesure du flux de sève brute dans le tronc des arbres. Ann. Sci. For. 42 (2), 193–200.

Helfter, C., Shephard, J.D., Martinez-Vilalta, J., Mencuccini, M., Hand, D.P., 2007. A noninvasive optical system for the measurement of xylem and phloem sap flow in woody plants of small stem size. Tree Physiol. 27, 169–179.

Kozlowski, T.T., Pallardy, S.G., 1997. Transpiration and plant water balance. Chapter 12 in Physiology of Woody Plants. Academic Press, pp. 269–308 (Second Edition).

Kumar, R., Hosseinzadehtaher, M., Hein, N., Shadmand, M., Krishna Jagadish, S.V., Ghanbarian, B., 2022. Challenges and advances in measuring sap flow in agriculture and agroforestry: a review with focus on nuclear magnetic resonance. Front. Plant Sci. https://doi.org/10.3389/fpls.2022.1036078.

Nadezhdina, N., Tributsch, H., Cermak, J., 2004. Infra-red images of heat field around a linear heater and sap flow in stems of lime trees under natural and experimental conditions. Ann. For. Sci. 61, 2023–2213.

Nadezhdina, N., Vandegehuchte, M.W., Steppe, K., 2012. Sap flux density measurements based on the heat field deformation method. Trees 26, 1439–1448.

Nagata, A., Kose, K., Terada, Y., 2016. Development of an outdoor MRI system for measuring flow in a living tree. J. Magn. Reson. 265, 129–138, 2016.

Marshall, D.C., 1958. Measurement of sap flow in conifers by heat transport. Plant Physiol. 33 (6), 385–396.

Poyatos, R., et al., 2021. Global transpiration data from sap flow measurements: the SAPFLUXNET database. Earth Syst. Sci. Data 13 (6), 2607–2649. https://doi.org/10.5194/essd-13-2607-2021.

Ratovoson, D., Huon, V., Costalat, V., Jourdan, F., 2011. Combined model of human skin - heat transfer in the vein and tissue: experimental and numerical study. Quant. InfraRed Thermogr. J. 8 (2), 165–186, 2011.

Sakuratani, T., 1981. A heat balance method for measuring water flux in the stem of intact plants. J. Agric. Met. 37, 9–17.

Serantoni, V., Jourdan, F., Louche, H., Sultan, A., 2021. Proposal for a protocol using an infrared microbolometer camera and wavelet analysis to study foot thermoregulation. Quant. InfraRed Thermogr. J. 18 (2), 73–91.

Sidi-Boulenouar, R., Reis, A., Native, lE., Buy, S., de Pellegars, P., Liu, P., Zanca, M., Goze-Bac, C., Barbat, J., Alibert, E., Verdeil, J.L., Gatineau, F., Bertin, N., Anand, A., Coillot, C., 2018. Homogenous static magnetic field coils dedicated to portable nuclear magnetic resonance for agronomic studies. J. Sens. Sens. Syst. 7, 227–234.

Steinberg, S., VanBavel, C.H.M., McFarland, M.J., 1989. A gauge to measure mass-flow rate of sap in stems and trunks of woody plants. J. Am. Soc. Hortic. Sci. 114, 466–472.

Swanson, R.H., Whitfield, W.A., 1981. A numerical analysis of heat pulse velocity theory and practice. J. Exp. Bot. 32, 221–239.

Tributsch, H., Nadezhdina, N., Cermak, J., 2006. Infrared images of heat fields around a linear heater in tree trunks: what can be learned about sap flow measurement? Ann. For. Sci. 63, 653–660.

Van As, H., Schaafsma, T., 1984. Non-invasive measurement of plant water flow by nuclear magnetic resonance. Biophys. J. 45, 46–472, 1984.

Vandegehuchte, M.W., Steppe, K., 2012. Sapflow+: a four-needle heat pulse sap flow sensor enabling nonempirical sap flux density and water content measurements. New. Phytol. 196, 306–317.

Vandegehuchte, M.W., Steppe, K., 2013. Sap-flux density measurement methods: working principles and applicability. Funct. Plant Biol. 40 (3), 213–223.

Wiedemann, A., Marañon-Jiménez, S., Rebmann, C., Herbst, M., Cuntz, M., 2016. An empirical study of the wound effect on sap flux density measured with thermal dissipation probes. Tree Physiol. 36 (12), 1471–1484.

Windt, C.W., Vergeldt, F.J., de Jager, P.A., Van As, H., 2006. MRI of long-distance water transport: a comparison of the phloem and xylem flow characteristics and dynamics in poplar, castor bean, tomato and tobacco. Plant Cell Environ. 29, 1715–1729.